Preparation of indole surface molecularly imprinted polymer by atom transfer radical emulsion polymerization and its adsorption performance

Yang Wenming
School of Materials Science and Engineering, Jiangsu University, Zhenjiang 212013, China

Cao Yang and Xu Xiaoling
School of the Environment, Jiangsu University, Zhenjiang 212013, China

Zhou Zhiping[a)]
School of Materials Science and Engineering, Jiangsu University, Zhenjiang 212013, China

Liu Lukuan and Xu Wanzhen[b)]
School of the Environment, Jiangsu University, Zhenjiang 212013, China

(Received 29 May 2013; accepted 16 August 2013)

The indole molecularly imprinted polymer (indole-MIP) was synthesized by atom transfer radical emulsion polymerization (ATREP). The novel adsorbent was used to adsorb indole from fuel oil. The indole-MIP had a high selectivity to indole, and the mass transfer limitations were overcome. The property and morphology of indole-MIP were described by a series of characterization methods. A great specific area and more pores of indole-MIP were shown. The static adsorption experiments display that equilibrium adsorption capacity of indole-MIP was 34.488 mg/g. The adsorption process was spontaneous by thermodynamic analysis, and a dense mass of indole was adsorbed onto indole-MIP at a proper low temperature (298 K). Pseudo-second-order kinetic model was more fitted with experimental data. Both Langmuir and Freundlich isotherm models were obeyed by adsorption isotherm test. The selective and competitive performances of indole-MIP were favorable, and the regeneration capacity was appreciable.

I. INTRODUCTION

Nitrogen oxide emitted into the atmosphere is the main substance to cause acid rain when the fuel oil product was used, and it will lead to environmental pollution and threat human health.[1] So it is very important to deeply remove nitrogen components from fuel oil. Generally, basic and nonbasic nitrogen are included in fuel oil, furthermore, indole and its derivatives are the primary nonbasic nitrogen. Recently, many denitrification technologies such as hydrodenitrogenation,[2] biological denitrification,[3] microwave denitrification,[4] and combination denitrification[5] have been applied to disposing nitrogen from fuel oil and made some achievements. However, these methods mentioned above are effective to remove the basic nitrogen compounds and less reliable to wipe off nonbasic nitrogen. Therefore, the key is how to remove nonbasic nitrogen effectively, and the stability of fuel oil will be maintained. Indole as typical nonbasic nitrogen has been paid more attention.

Molecular imprinting technique (MIT) is a simple and efficient method to prepare polymers with specific recognition sites for the certain target molecule.[6–8] Many outstanding advantages[9] of molecularly imprinted polymer (MIP) are shown, so it has been a promising candidate for chromatographic analysis,[10] solid-phase extraction,[11] antibody mimics,[12] biomimetic catalysis,[13] sensors,[14–17] drug development,[18] and other applications. Since the surface MIP has a high binding capacity and a fast mass transfer, it has been used to overcome some drawbacks such as poor accessibility of the binding sites, low binding capacity and so on.[19–21]

Nowadays, the MIP prepared by free radical polymerization (FRP) has been reported by many works.[22] The controlled "living" radical polymerization (CRP) techniques create a whole new dimension in the synthesis of polymeric system which is unable to propagate and self-terminate chain reaction.[23–25] Therefore, the extent of CRP relies on setting up a dynamic equilibrium between active and dormant species. The probability of bimolecular termination reaction is minimized, and the radical polymerization behaves as a living system.[26,27] As one of the most efficient and powerful methods in CRP techniques, atom transfer radical polymerization (ATRP) with characteristics of predictable molecular weights, mild polymerization conditions, remarkable tolerance of functional groups, and very diverse polymeric materials has attracted more considerable attention.[28] The ATRP has been applied in surface imprinting technology by grafting polymer on

Address all correspondence to these authors.
[a)]e-mail: zhouzp@ujs.edu.cn
[b)]e-mail: xwz09@ujs.edu.cn
DOI: 10.1557/jmr.2013.256

 © Materials Research Society 2013

https://doi.org/10.1557/jmr.2013.256 Published online by Cambridge University Press

the supporter surface. Because the microspheres will process reactive halogen groups on its surface, and it ensures that the cross-linked polymer was grafted to the substrate by covalent bond.[29] The mechanism of ATRP is simply described in Fig. 1.[30–32]

In our work, we combined the surface MIT and atom transfer radical emulsion polymerization (ATREP) to prepare indole-MIP for selective adsorption of indole from fuel oil. It is important to note that the SiO_2 modified by MPS (MPS-SiO_2) was selected as a supporter, and indole as template, 4-vinylpyridine (4VP) as functional monomer, ethylene glycol dimethacrylate (EGDMA) as cross-linker, copolymer monomer. The kinetics, isotherms, and thermodynamic analysis have been performed to study the adsorption mechanism of indole onto indole-MIP. The structure and morphology of indole-MIP were characterized by nitrogen adsorption, infrared spectrum, scanning electron microscopy (SEM), and thermogravimetric analysis (TGA).

II. EXPERIMENTAL

A. Materials and instrument

4-vinylpyridine (4VP, 99.5%), indole (98.5%), 3-methylindole (98%), quinoline (99%), benzothiophene (BT, 99%), ethylene glycol dimethacrylate (EGDMA, 98%), *n*-octane (AR) were supplied by Sigma-Aldrich Chemical Company (St. Louis, MO). Tetradecane (99.9%), toluene (AR), and acetone (AR) were obtained from Nanjing Union Silicon chemical (Nanjing, China). CuCl (AR), N,N,N′,N″, N″-pentamethyl diethylenetriamine (PMDETA, 98%), γ-methacryloxypropyltrimethoxysilane (MPS, 97%), ethyl-2-bromoisobutyrate (EBiB), methanol (MeOH, AR), ammonia (AR), ethanol (AR), and acetic acid (AcOH, AR) were received from the Sinopharm Chemical Reagent (Shanghai, China). Polysorbate-(60) (Tween 60) and tetraethyl orthosilicate were purchased from Aladdin Reagent Co., Ltd. (Shanghai, China).

Flowsorb II 2300 manufactured by Micromeritics Instrument Corporation, Norcross, GA. NICOLET NEXUS 470 Fourier transform infrared spectrometry (FTIR) was obtained from Thermoelectric (Thermo Nicolet Corporation, Madison, WI). S-4800 field emission SEM was purchased from Hitachi (Tokyo, Japan). STA449C TGA was purchased from Netstal (Bayerische, Germany). AVANCE II 400 MHz H^1-nuclear magnetic resonance (H^1-NMR) was obtained from Bruker (Switzerland). Agilent 7890A gas chromatography containing a flame ionization detector was manufactured from Agilent (Santa Clara, CA).

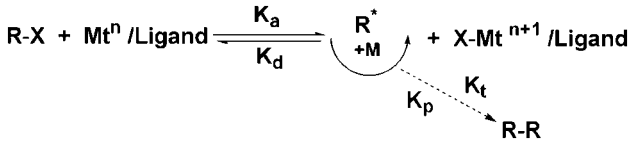


FIG. 1. Schematic illustration of ATRP.

B. Synthesis of Indole-MIP and nonimprinted polymer by ATREP

1. Preparation of SiO_2 particles

The SiO_2 particles were obtained at 45 °C in the mixture with molar concentrations of tetraethyl orthosilicate, ammonia, and deionized water of 0.3 mol/L, 2.5 mol/L, and 15 mol/L, respectively. The tetraethyl orthosilicate was dropwise added into the mixture of ethanol, deionized water, and ammonia. The resulting substance was filtered, washed, and dried before use.

2. Synthesis of modified SiO_2 particles

The obtained SiO_2 and 6 mL of MPS were dispersed in 50 mL of dry toluene in a sealed flask. Under nitrogen environment, the reaction condition was conducted at 114 °C with continuous stirring for 24 h. The products were filtered and washed with toluene, acetone, and ethanol in sequence and then dried in a vacuum at 60 °C. The SiO_2 modified by MPS (SiO_2@MPS) was achieved.

3. Synthesis of indole-MIP and NIP

The indole-MIP was prepared by ATREP according to the following procedures: at first, SiO_2@MPS (1 g), indole (0.5 mmol), 4VP (2 mmol), EGDMA (6 mmol) were added into a 50 mL of round-bottom flask with water (30 mL) and Tween 60 (0.45 g). The mixture was processed by ultrasonic dispersion for 20 min and then deoxygenated with nitrogen for 15 min. The prepolymerization was carried out at room temperature with continuous magnetic stirring in nitrogen environment for 6 h. After that, PMDETA (0.1 mmol), CuCl (0.1 mmol) purified by acetic acid, and EBiB (0.15 mmol) were quickly transferred into the reaction system under the protection of nitrogen. The flask containing the mixture was immersed in a constant temperature oil bath at 60 °C with continuous stirring for 24 h. The obtained products were filtered and successively washed with ethanol and acetone to remove the unreacted substances. Finally, the indole template was removed from indole-MIP by a mixing methanol/acetic acid solvent (9:1, v/v) for 72 h. The indole-MIP on the SiO_2 particle surface by ATREP was synthesized successfully and dried in a vacuum at 60 °C.

The corresponding nonimprinted polymer (NIP) was prepared as a blank using the same methods under the identical conditions but indole template was omitted in the polymerization process.

C. Characterizations of indole-MIP and NIP

The Flowsorb II 2300 was used to measure the specific area (m^2/g), the pore volume (cm^3/g), and pore diameter (Å). The FTIR was used to obtain infrared spectrogram with KBr as tableting between 4000 cm^{-1}

https://doi.org/10.1557/jmr.2013.256 Published online by Cambridge University Press

and 400 cm^{-1}. The SEM was used to observe the morphological characteristics and structures of polymers. TGA was used to measure the components and thermal stability, the sample was heated under nitrogen atmosphere from room temperature to 1000 °C with a heating rate of 10 °C. The H^1-NMR was used to obtain the spectrum of interaction between functional monomer and template molecule, and deuterated acetone was selected as the solvent.

D. Performance test of indole-MIP

The Agilent 7890A gas chromatography [equipped with a flame ionization detector (GC-FID)] was used to detect the residuary concentration of indole to obtain the rebinding capacity of indole onto indole-MIP in adsorption tests.

1. Test of adsorption kinetics

To investigate the adsorption equilibrium and the adsorption rate of indole-MIP toward indole, three group parallel tests have been carried out in simulate oil (*n*-octane as a solvent, indole as a solute) with the initial concentration of 300 mg/L at different temperatures (298, 308, and 318 K), respectively. Specific operation was as follows: first, 10 mg of indole-MIP was added into centrifuge tubes with 5 mL simulate oil, and then the tubes were shaken in a vapor-bathing constant temperature vibrator at preset temperatures for predetermined time intervals, respectively. Concentrations of indole that remained in the supernatant were detected by GC after centrifugation.

2. Test of adsorption isotherms

To explore the effect of concentration on adsorption capacity and equilibrium constant, 10 mg of indole-MIP was added into test tubes containing 5 mL simulate oil solution with different initial concentrations (from 100 to 800 mg/L). Then the test tubes respectively were shaken in a vapor-bathing constant temperature vibrator at preset temperatures (298, 308, and 318 K) for 3 h. The concentrations of the remaining indole in the supernatant were detected in the same way as adsorption kinetics.

3. Test of selective and competitive adsorption

To study the selectivity of indole-MIP toward indole, the experiment was carried out in four different solutions of 300 mg/L, which respectively were indole, 3-methylindole, quinoline, and BT. However, the competitive adsorption test of the indole-MIP was conducted in a 300 mg/L mixture containing the above four kinds of substances. The operations of both parts were similar to that of adsorption isotherms, and the adsorption processes were allowed to conduct at 298 K for 3 h.

III. RESULTS AND DISCUSSION

A. Preparation of indole-MIP

The indole-MIP grafted on the SiO_2 surface had a high adsorption capacity due to the large specific area. The SiO_2 was modified by grafting MPS, so the polymerizable double bonds were introduced to carry out the polymerization reaction. The 4VP was chosen as the functional monomer based on the consideration that hydrogen bond was formed between 4VP and indole, and multiple hydrogen-binding sites could be provided. Furthermore, the mol ratio of functional monomer and template was 4:1. The EGDMA was chosen as cross-linker, and the polymerization was initiated by the reaction between the EBiB and transition metal complex (Cu^+/PMDETA). In our experiment, the synthesis of indole-MIP by the ATREP was carried out in the water containing the surfactant Tween 60. The emulsion polymerization was adopted to prepare nanoparticles, which could be advantageous to mass transfer and enhance adsorption capacity. The schematic illustration of polymerization is shown in Fig. 2.

B. Structural characterization of indole-MIP and NIP

1. Nitrogen adsorption analysis

The Brunauer–Emmett–Teller (BET) equation was used to measure the specific area (m^2/g) of indole-MIP and NIP. The pore volume (cm^3/g) and pore diameter (Å) were analyzed by the Barrett–Joyer–Halendal (BJH) model. The resulting data are shown in Table I. It is seen that the pore property values of indole-MIP were similar to those of NIP. However, the specific area of indole-MIP was larger than that of NIP. Therefore, compared with NIP, more pores on indole-MIP were shown to be present. It was attributed to the removal of template indole, and the imprinting sites were remained. Therefore, the indole-MIP had the favorable spaces for indole, and this could promote the interaction between indole-MIP and indole.

2. Infrared spectrum analysis

The FTIR spectra of the SiO_2 particles, SiO_2@MPS, and indole-MIP respectively are shown in Fig. 3. The main functional groups of each step in polymerization were confirmed by the corresponding infrared adsorption peaks. The presence of hydroxyl group was proven by characteristic adsorption peak of H–O at 3449 cm^{-1} in spectral line a. Both the stretching vibration absorption peaks of C=O and C=C respectively were displayed at around 2977 cm^{-1} and 1728 cm^{-1}; it verifies that the SiO_2 was modified by MPS via the covalent bond in spectral line b. In addition, from spectral line c, the deformation vibration peak of C=N found at 1605 cm^{-1} proves that 4VP was grafted successfully. All the above results reveal that the surface MIP was obtained by ATREP.

https://doi.org/10.1557/jmr.2013.256 Published online by Cambridge University Press

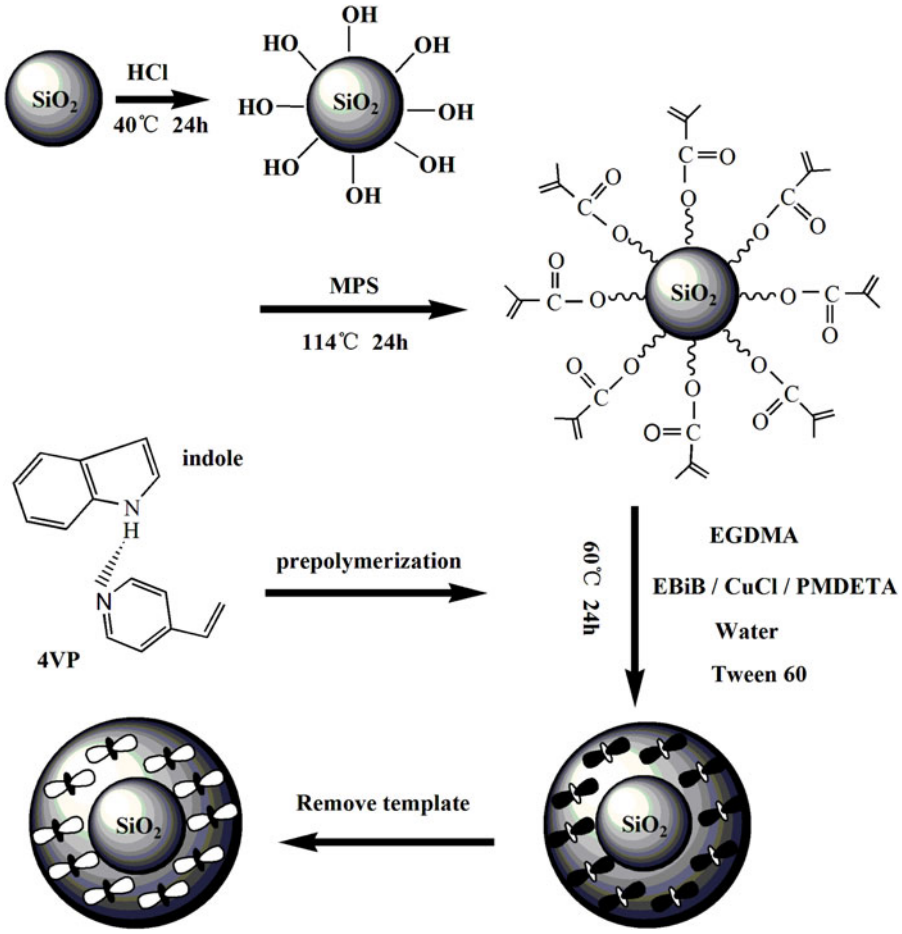


FIG. 2. Schematic for the preparation of indole-MIP.

3. SEM analysis

The morphology of indole-MIP and NIP is displayed in Fig. 4. Compared with NIP (b), the rougher surface, more pores, and larger surface area of indole-MIP (a) are displayed.

TABLE I. Pore properties of indole-MIP and NIP.

Polymer	Specific area (m^2/g)	Pore volume (cm^3/g)	Pore diameter (Å)
Indole-MIP	141.305	0.389	81.247
NIP	110.827	0.372	80.486

4. Thermogravimetric analysis

The TGA curve of indole-MIP is given in Fig. 5. The mass of SiO_2 particles and the imprinting layer was measured by TGA. The indole-MIP almost had a constant weight when the temperature was increased from 25 °C to 100 °C. The result mainly suggests that the polymer was dried absolutely without moisture evaporation. A percent of 56.8 dropped in quality of indole-MIP when the temperature was rising and over 250 °C. The lost mass was identified as the polymer coating at the SiO_2 particle surface. Thus, the rest of the substance was SiO_2 particles, which could not be melted until the temperature reached 1670 °C, and it was about 43.2% of the total mass.

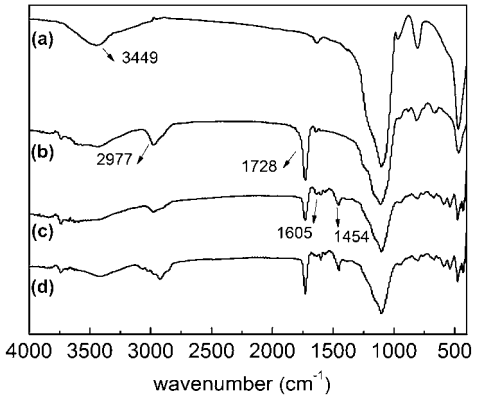


FIG. 3. FTIR spectra of (a) SiO_2, (b) MPS-SiO_2, and (c) indole-MIP.

https://doi.org/10.1557/jmr.2013.256 Published online by Cambridge University Press

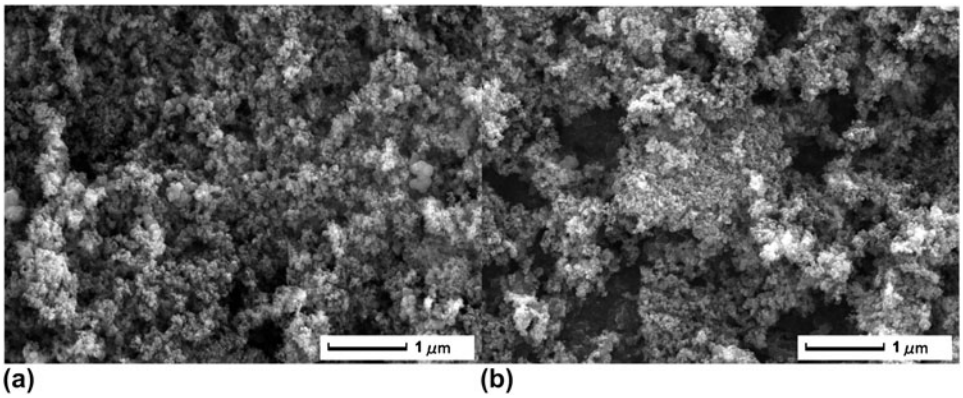


FIG. 4. The SEM images of (a) indole-MIP and (b) NIP.

5. H^1-NMR analysis

The H^1-NMR lines of indole, 4VP, and the complex between indole and 4VP are represented in Fig. 6. The different line widths and chemical shifts indicated the presence of different types of hydrogen. For line a, a larger line width has been found at the chemical shift $\delta = 10.2$ ppm for hydrogen engaged in nitrogen of indole, and the hydrogens located on aromatic heterocyclic rings and benzene ring of indole were shown approximately from 7.6 to 6.5 ppm. Furthermore, $\delta = 2.0$ ppm represented the solvent peak of deuterated acetone. For spectral line b, the hydrogens engaged in double bond of 4VP were shown at chemical shifts $\delta = 6.8$, 6.1, and 5.5 ppm. The peaks at $\delta = 8.5$ and 7.4 ppm could be assigned to the hydrogens located on aromatic of 4VP. As is shown in spectral line c, the peak at chemical shift $\delta = 10.3$ was low, a slight change has been shown. Meanwhile, the chemical shifts of other lines were almost maintained in the complex. The result shows that the chemical reaction was not carried out between template indole and functional monomer 4VP, and the interaction force could be hydrogen bond and intermolecular force, etc.

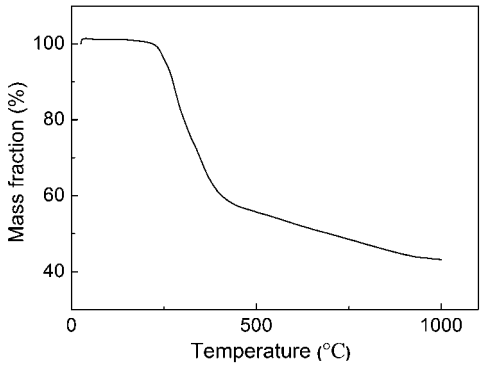


FIG. 5. TGA curve of indole-MIP.

C. Adsorption performance of indole-MIP

1. Analysis of adsorption kinetics

The fitting curves of Weber–Morris diffusion equation, pseudo-first-order and pseudo-second-order models are shown in Fig. 7. It is seen that the adsorption curves were steep in the initial phase and then got flattened after 30 min. An increase in adsorption rate of indole-MIP toward indole was shown during the first 30 min. As time progresses, the adsorption rate decreased slowly until the equilibrium was achieved. The result could be attributed to a large number of unoccupied sites on indole-MIP surface at the beginning of the adsorption process. A higher affinity, weaker steric hindrance, and less mass resistance for inodol-MIP toward indole were displayed. Subsequently, most of the binding sites were occupied by indole molecules so that the adsorption rate was decreased and the equilibrium was reached. Because of the hydrogen bond between the template and the functional monomer, the adsorption equilibrium was obtained in a short time even at different temperatures.

The adsorption capacity was calculated according to Eq. (1).

$$q_t = (C_0 - C_t)V/m \quad , \tag{1}$$

where q_t (mg/g) represents the amount of adsorbed indole at time t; C_0 and C_t are the concentration of indole at initial and time t, respectively; V and m respectively are the volume of simulate oil and mass of indole-MIP.

The data obtained from adsorption experiments were fitted with the Weber–Morris diffusion equation, pseudo-first-order and pseudo-second-order equations to investigate the mechanism and interaction in the adsorption process. The Weber–Morris diffusion equation can be given by Eq. (2),

$$q_t = k_i t^{1/2} + k_d \quad , \tag{2}$$

where k_i and k_d (mg/g/min) respectively stand for diffusion coefficient and diffusion boundary constant and can be calculated from the plot of q_t versus $t^{1/2}$.

https://doi.org/10.1557/jmr.2013.256 Published online by Cambridge University Press

The pseudo-first-order model[33] can be expressed as follows:

$$\ln(q_e - q_t) = \ln(q_e) - k_1 t \quad , \tag{3}$$

where the q_e (mg/g) and q_t (mg/g) are the adsorbed indole amount at equilibrium and time t, respectively; k_1 is the adsorption rate constant of pseudo-first-order.

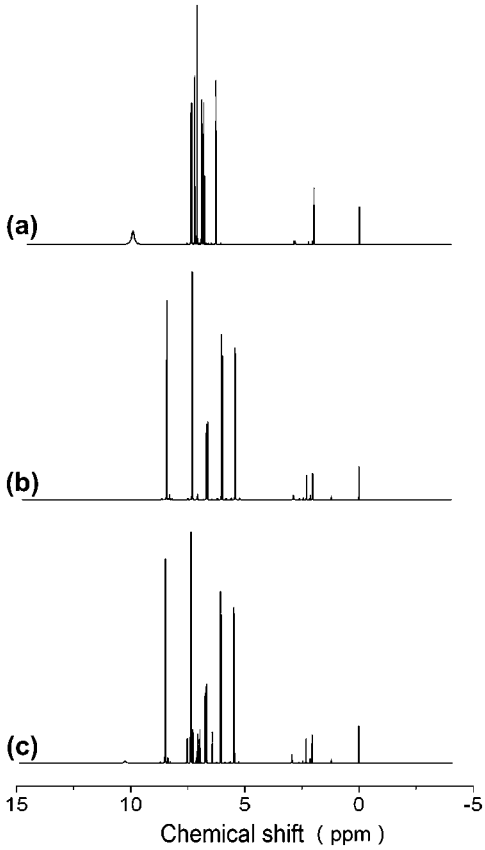


FIG. 6. H^1-NMR spectra of (a) indole, (b) 4VP, and (c) complex of indole and 4VP.

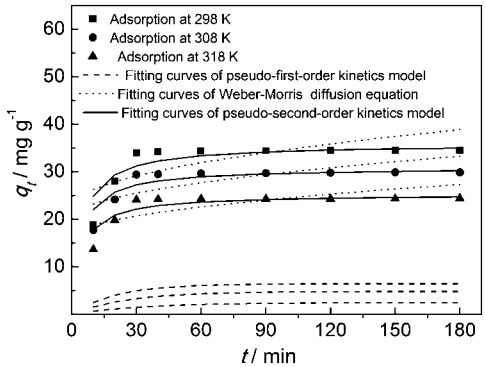


FIG. 7. Kinetic adsorption and fitting curves of indole-MIP toward indole with 500 mg/L initial concentration at different temperatures.

The pseudo-second-order model[34] can be expressed as:

$$t/q_t = 1/k_2 q_t^2 + t/q_e \quad , \tag{4}$$

where k_2 is the adsorption rate constant of pseudo-second-order.

The adsorption rate constants and linear regression values of these models are summarized in Table II. It is obvious to find that the regression coefficient values (R^2) of the pseudo-second-order model were higher than those of the pseudo-first-order model and the Weber–Morris diffusion equation. The values of R^2 were all above 0.99 even at different temperatures, which suggested only a slight difference between the experimental and theoretical values of q_e for the pseudo-second-order model. And compared with the other two models, the adsorption process of indole-MIP toward indole was more palatable to the pseudo-second-order model. The chemical adsorption was dominant and controlled the rate of interaction in the process of rebinding indole.

2. Analysis of adsorption isotherms

Adsorption isotherm experiments were performed at different temperatures (298, 308, and 318 K) with indole initial concentrations ranging from 100 to 800 mg/L. The fitting curves of experimental results are displayed in Fig. 8. As shown in Fig. 8, the adsorption capacity increased with increasing initial concentrations. It was due to the intensive indole molecules contained in unit volume, and it was easier to be combined with indole-MIP. However, with increasing temperatures, there was a decrease in the binding capacity. The reason for this phenomenon was the weak hydrogen bond force between 4VP and indole at a high temperature. Therefore, an appropriate low temperature could enhance the hydrogen bonding interaction and promote the adsorption of indole onto indole-MIP.

TABLE II. Kinetic parameters of the adsorption process of indole-MIP toward indole.

Models	Parameters	298 (K)	308 (K)	318 (K)
Pseudo-first-order model	$q_{e,exp}$ (mg/g)	34.488	29.853	24.410
	$q_{e,cal}$ (mg/g)	6.413	4.794	2.479
	$k_1 \times 10^{-3}$ (min^{-1})	48.823	38.921	29.709
	Δq (%)	33.238	70.304	68.976
	R^2	0.860	0.806	0.615
Pseudo-second-order model	$q_{e,cal}$ (mg/g)	35.842	30.864	25.253
	$k_2 \times 10^{-3}$ (g/mg min)	6.313	8.113	9.481
	Δq (%)	16.834	13.577	7.536
	R^2	0.998	0.998	0.998
Weber–Morris diffusion equation	K_i	1.2243	0.9778	0.8374
	K_d	22.432	20.142	16.110
	R^2	0.4908	0.5099	0.4848

https://doi.org/10.1557/jmr.2013.256 Published online by Cambridge University Press

The equilibrium adsorption capacity was obtained according to the following equation:

$$q_e = (C_0 - C_e)V/m \quad , \tag{5}$$

where q_e (mg/g) and C_e respectively are the adsorption capacity of indole-MIP (mg/L) and concentration of indole at equilibrium.

Here, the experimental data were respectively analyzed by Langmuir isotherm model and Freundlich isotherm model. The nonlinear expression of the Langmuir model[35] was given by the following Eq. (6):

$$C_e/q_e = C_e/q_m + 1/(q_m K_L) \quad , \tag{6}$$

where q_e is the equilibrium adsorption amount of indole-MIP (mg/g); C_e is the equilibrium concentration of indole (mg/L); q_m (mg/g) is the calculation of the saturation adsorption capacity of the indole-MIP; K_L is the Langmuir constant representing the affinity constant.

The Freundlich isotherm model[36] was displayed as Eq. (7):

$$\log q_e = \log C_e/n + \log K_F \quad , \tag{7}$$

where K_F is the Freundlich constant.

The correlation coefficients of both isotherm models are displayed in Table III. According to the high coefficient values (R^2), both Langmuir isotherm model and Freundlich isotherm model were relatively fitted with experimental values. Thus, the process of indole adsorbed onto indole-MIP obeyed these two isotherm models well.

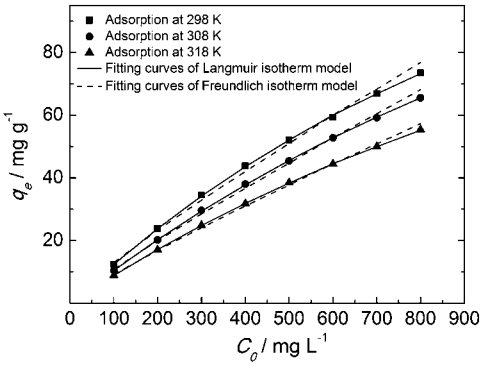


FIG. 8. Adsorption isotherms and fitting curves of indole-MIP toward indole with different initial concentrations at different temperatures.

The monolayer adsorption for indole-MIP toward indole was proved, and the adsorption was nonuniform. Both the chemical adsorption and the physical adsorption were included in the interaction process. The chemical adsorption shows the special adsorption and recognition of imprinting sites toward indole.

3. Adsorption thermodynamics

The standard enthalpy change (ΔH°),[37] the standard free energy change (ΔG°)[38] and the standard entropy change (ΔS°)[39] were chosen to describe the thermodynamic characteristics during the adsorption process. These parameters were calculated by following Eqs. (8) and (9):

$$\ln K_c = -\Delta H^\circ/RT + \Delta S^\circ/R \quad , \tag{8}$$

$$\Delta G = -RT \ln K_c \quad , \tag{9}$$

where K_c is a distribution constant (mL/g) obtained by the intercept of the straight line, which plotting $\ln(q_e/C_e)$ versus q_e and extrapolating q_e to zero; T is the absolute temperature (K); R is the gas constant (8.3145 J/mol/K).

These thermodynamic parameters for the adsorption process of indole onto indole-MIP are displayed in Table IV. The adsorption process was spontaneous within the investigated temperatures by a negative ΔG° value. The adsorption process was exothermic; this could be confirmed by a negative value of ΔH°, and the weak adsorption capacity at a high temperature was further proven. The thermodynamic quotient reduction was shown in the interaction process by a negative ΔS°.

4. Selectivity and competitive adsorption of indole-MIP and NIP

According to the similar size and functional group, reference substances of indole such as 3-methylindole, quinoline, and BT were chosen to explore the selective and competitive adsorption of indole-MIP and NIP toward indole. The chemical structures of the above-mentioned substances are shown in Fig. 9. Compared with template indole, BT has a similar size but the functional group is different. However, 3-methylindole and quinoline have identical functional groups to indole while having differences in size.

TABLE III. Parameters of the Langmuir and Freundlich isothermal equations.

		Langmuir parameters			Freundlich parameters		
T (K)		q_m (mg/g)	K_L (L/mg)	R^2	K_F	n	R^2
Indole-MIP	298	192.3077	0.00094	0.9980	0.39930	1.23213	0.9960
	308	208.3333	0.00069	0.9986	0.27127	1.17689	0.9974
	318	178.5714	0.00065	0.9985	0.22085	1.17550	0.9983

https://doi.org/10.1557/jmr.2013.256 Published online by Cambridge University Press

The selectivity adsorption experiment for each of adsorbates was carried out under identical conditions. The equilibrium adsorption capacity of indole-MIP and NIP toward indole and analogs is shown in Fig. 10. The results indicate that indole-MIP had a higher binding capacity toward indole than toward other analogs. It means that the indole-MIP had a better selectivity for indole. This phenomenon was attributed to the imprinting effect, which could recognize the molecular size, structure, and functional group by imprinting sites. In addition, the adsorption capacity of indole-MIP toward 3-methylindole was more than toward quinoline and BT due to the identical interaction of 3-methylindole and indole with 4VP. The indole-MIP toward BT had the minimum adsorption capacity, because the interaction between BT and 4VP is weak, even though BT has a similar size to indole. Meanwhile, it is seen that the binding capacity of indole-MIP toward indole and its analogs was higher than that of NIP because of the imprinted sites and pore structures on the indole-MIP surface. In the whole adsorption process, the hydrogen bond between nitrogen of 4VP and hydrogen of indole was the main driving force and plays an important role. However, the adsorption process was complex, besides the hydrogen bond interaction, the electrostatic interaction and other interactions such as the synergistic effect of shape complementarity were also involved in noncovalence interactions between the functional monomer and the target.

TABLE IV. Thermodynamic parameters for the adsorption process of indole-MIP toward indole.

T (K)	K_c	$\Delta G°$ (kJ/mol)	$\Delta H°$ (kJ/mol)	$\Delta S°$ (J/mol/K)
298	5.5554	−4.2487		
308	5.2956	−4.2686	−4.2878	−180.0885
318	4.9816	−4.2456		

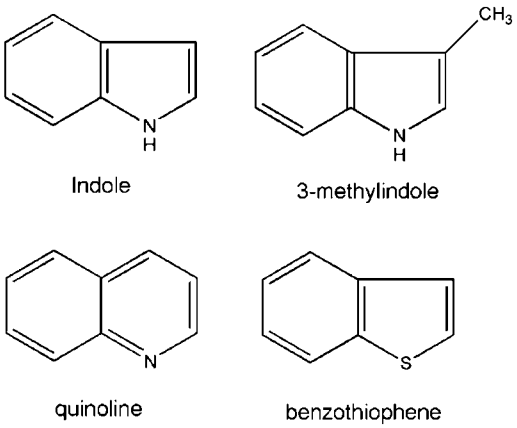


FIG. 9. Chemical structures of the indole, 3-methylindole, quinoline, and BT.

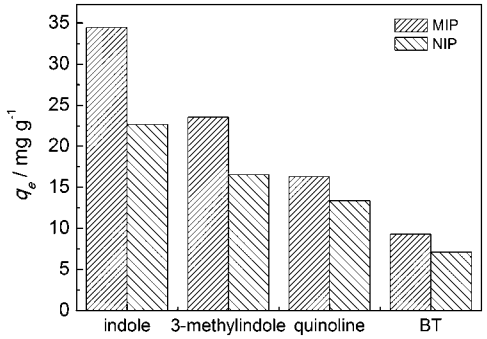


FIG. 10. Selective adsorption capacity toward indole, 3-methylindole, quinoline, and BT of indole-MIP and NIP.

To further explore the rebinding capacity of the indole-MIP and NIP toward indole, the experiment was carried out in mixing solution containing indole and three kinds of analogs. The purpose of competitive adsorption was to test the interference of analogs to the adsorption of indole-MIP toward indole. The adsorption capacities of indole-MIP and NIP were evaluated by some parameters such as K_d, k, and k', which were calculated by equations as follows.

The distribution coefficients of the selectivity adsorption toward indole, 3-methylindole, quinoline, and BT were calculated according to Eq. (10):

$$K_d = q_e/C_s \quad , \tag{10}$$

where K_d (mL/g) is the distribution coefficient, q_e (mg/g) and C_s (mg m/L) are the equilibrium adsorption capacity and the concentration of the adsorbate, respectively.

The selectivity coefficient of indole toward its competitor (marked as B) could be obtained by the following Eq. (11):

$$k = K_d(\text{indole})/K_d(\text{B}) \quad , \tag{11}$$

where k is the selectivity coefficient, B represents 3-methylindole, quinoline, and BT, respectively.

The relative selectivity coefficient k' could be figured out with Eq. (12),

$$k' = k_{MIP}/k_{NIP} \quad , \tag{12}$$

where k' is the relative selectivity coefficient.

The resulting data are listed in Table V, and the illustration by comparison is shown in Fig. 11. The high adsorption

TABLE V. Selective recognition parameters of indole-MIP and NIP.

	MIP		NIP		
Mixed solution	K_d	k	K_d	k	k'
Indole	92.025	...	52.274	...	...
3-methylindole	30.118	3.055	28.341	1.844	1.657
Quinoline	8.627	10.667	7.561	6.914	1.543
BT	6.746	13.641	5.612	9.315	1.464

https://doi.org/10.1557/jmr.2013.256 Published online by Cambridge University Press

capacity of indole onto indole-MIP even in the mixed solution is shown. The reason is that indole-MIP with a great deal of specific cavities had a specific molecular recognition ability and high binding affinity to indole. However, compared with Fig. 10, the rebinding capacity of indole-MIP to indole had a slight decrease, and it could be attributed to the competition between indole and its analogs on binding sites. Even in this situation, the adsorption capacity of indole onto indole-MIP was obviously higher than onto NIP. It indicated the high selectivity of indole-MIP and the significant effect of imprinting sites.

The distribution coefficients, selectivity coefficients, and relative selectivity coefficients are shown in Table V. Both K_d and k of indole-MIP were greater than those of NIP; this provides a further explanation to the selectivity of indole-MIP. Imprinting sites obtained onto indole-MIP were sufficient to illustrate the difference between indole-MIP and NIP in adsorption capacity. The k'(indole) was obviously finer than k'(3-methylindole, quinoline, and BT). All the results clearly reveal that indole-MIP with excellent recognition and binding affinity to template indole was achieved successfully by ATREP.

5. Regeneration of indole-MIP

To study the regeneration and stability of indole-MIP, the cycling tests were carried out in the concentration of 300 mg/L of simulate oil.[40] The mixture of methanol and acetic acid (9/1, V/V) was selected as an eluent. The adsorption operation was conducted according to adsorption isotherm experiment at 298 K for 3 h. The results of five regeneration cycles are shown in Fig. 12. After five cycles of adsorption and elution, the adsorption capacity of indole-MIP dropped by 6.59 mg/g compared with initial adsorption capacity. It indicates that the indole-MIP prepared by ATREP had a perfect reusability.

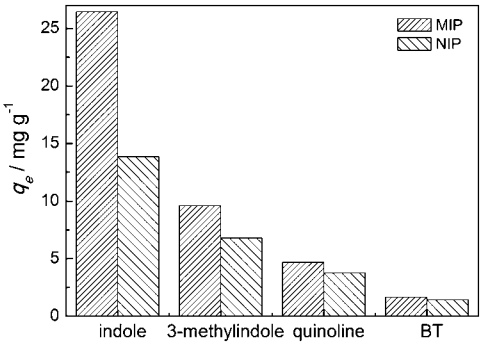


FIG. 11. Competitive adsorption capacity toward indole, 3-methylindole, quinoline, and BT of indole-MIP and NIP.

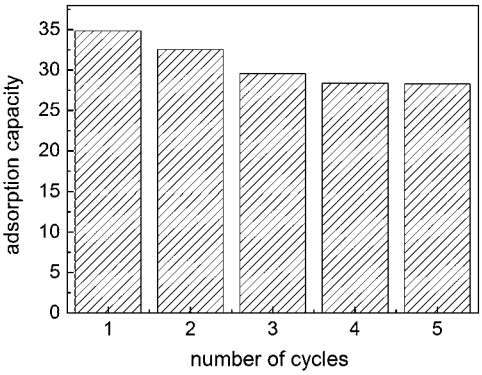


FIG. 12. Regeneration of adsorption indole onto indole-MIP.

IV. CONCLUSION

In our work, a novel surface MIP was synthesized by ATREP with 4VP as the functional monomer and SiO_2@MPS as the matrix. Nitrogen adsorption, FTIR, and SEM were used to characterize the structures and morphology of indole-MIP and NIP. The results show that indole-MIP was provided with the rougher surface and more pores. Meanwhile, the thermostability of indole-MIP was explored from room temperature to 1000 °C by TGA, and the interaction between indole and 4VP was detected by H^1-NMR. Adsorption experiment data show that the process of indole adsorbed onto indole-MIP was spontaneous, and the pseudo-second-order model was suitable to describe the adsorption performance. Both Langmuir and Freundlich isotherm models were obeyed by adsorption isotherm test. Furthermore, the adsorption equilibrium was reached in 30 min, and an appropriate low temperature could promote the rebinding capacity. This was attributed to the weak binding affinity of hydrogen bond between functional monomer and template at a high temperature. In addition, it could be seen that adsorption capacity increased with the increasing initial concentration. The adsorption property tests show that indole-MIP was able to selectively recognize and adsorb indole from simulate oil, and the reused performance was excellent. From the discussion, the preparation of indole-MIP for selective adsorption indole by ATREP was feasible and effective. And for all above, the combination of ATREP and surface imprinting technique could be used in the developed removal of a harmful substance from fuel oil and other fields.

ACKNOWLEDGMENTS

This work is subsidized by the National Natural Science Fund (Grant Nos. 21106056 and 21174057), Jiangsu Natural Science Fund of China (Grant No. BK2011512), a project funded by the Priority Academic Program Development of Jiangsu Higher Education Institutions (PAPD), Senior Talent Foundation of Jiangsu University (Grant No. 09JDG048), and Scientific Research Foundation of Jiangsu University (Grant Nos. Y11A133 and Y10A035).

https://doi.org/10.1557/jmr.2013.256 Published online by Cambridge University Press

REFERENCES

1. J.G.C. van Amsterdam, A. Hollander, J.D. Snelder, P.H. Fischer, H. van Loveren, J.G. Vos, A. Opperhuizen, and P.A. Steerenberg: The effect of air pollution on exhaled nitric oxide of atopic and nonatopic subjects. *Nitric Oxide* **3**, 492 (1999).
2. C.E. Xiang, Y.M. Chai, Y.Q. Liu, and C.G. Liu: Mutual influences of hydrodesulfurization of dibenzothiophene and hydrodenitrogenation of indole over NiMoS/γ-Al_2O_3 catalyst. *J. Fuel Chem. Technol.* **36**, 684 (2008).
3. H.B. Cheng, M. Kumar, and J.G. Lin: Interpretation of redox potential variation during biological denitrification using linear non-equilibrium thermodynamic model. *Int. Biodeterior. Biodegrad.* **67**, 28 (2012).
4. S.C. Ma, Y.J. Jin, X. Jin, J.J. Yao, B. Zhang, S. Dong, and R.X. Shi: Influences of co-existing components in flue gas on simultaneous desulfurization and denitrification using microwave irradiation over activated carbon. *J. Fuel Chem. Technol.* **39**, 460 (2011).
5. K. Kimura, M. Nakamura, and Y. Watanabe: Nitrate removal by a combination of elemental sulfur-based denitrification and membrane filtration. *Water Res.* **36**, 1758 (2002).
6. W.E. Mahmoud, Y.C. Chang, A.A. Al-Ghamdi, and F. Al-Marzouki: Encapsulation of β-galactosidase from Aspergillus oryzae based on "fish-in-net" approach with molecular imprinting technique. *Polym. Compos.* **34**, 299 (2013).
7. F. Deng, Y. Li, X. Luo, L. Yang, and X. Tu: Preparation of conductive polypyrrole/TiO_2 nanocomposite via surface molecular imprinting technique and its photocatalytic activity under simulated solar light irradiation. *Colloids Surf., A* **395**, 183 (2012).
8. B.J. Gao, S. Liu, and Y. Li: Preparation and recognition performance of uric acid-imprinted material prepared with novel surface imprinting technique. *J. Chromatogr. A* **1217**, 2226 (2010).
9. F. Puoci, F. Lemma, G. Cirillo, M. Curcio, O.I. Parisi, U.G. Spizzirri, and N. Picci: New restricted access materials combined to molecularly imprinted polymers for selective recognition/release in water media. *Eur. Polym. J.* **45**, 1634 (2009).
10. L.I. Andersson: Molecular imprinting: Developments and applications in the analytical chemistry field. *J. Chromatogr. B* **745**, 3 (2000).
11. C. He, Y. Long, J. Pan, K. Li, and F. Liu: Application of molecularly imprinted polymers to solid-phase extraction of analytes from real samples. *J. Biochem. Biophys. Methods* **70**, 133 (2007).
12. L. Ye and K. Mosbach: Molecularly imprinted microspheres as antibody binding mimics. *React. Funct. Polym.* **48**, 149 (2001).
13. R. Say, M. Erdem, A. Ersoz, H. Turk, and A. Denizli: Biomimetic catalysis of an organophosphate by molecularly surface imprinted polymers. *Appl. Catal., A* **286**, 221 (2005).
14. J. Li, F. Jiang, Y. Li, and Z. Chen: Fabrication of an oxytetracycline molecular-imprinted sensor based on the competition reaction via a GOD-enzymatic amplifier. *Biosens. Bioelectron.* **26**, 2097 (2011).
15. R.G. Liang, R.M. Zhang, and W. Qin: Potentiometric sensor based on molecularly imprinted polymer for determination of melamine in milk. *Sens. Actuators, B* **141**, 544 (2009).
16. X.W. Kan, Z.L. Xing, A.H. Zhu, Z. Zhao, G.L. Xu, C. Li, and H. Zhou: Molecularly imprinted polymers based electrochemical sensor for bovine hemoglobin recognition. *Sens. Actuators, B* **168**, 395 (2012)
17. N. Wu, L. Feng, Y.Y. Tan, and J.M. Hu: An optical reflected device using a molecularly imprinted polymer film sensor. *Anal. Chim. Acta* **653**, 103 (2009).
18. X. Shi, A. Wu, G. Qu, R. Li, and D. Zhang: Development and characterisation of molecularly imprinted polymers based on methacrylic acid for selective recognition of drugs. *Biomaterials* **28**, 3741 (2007).
19. B.J. Gao, J.H. Lu, Z.P. Chen, and J. Guo: Preparation and recognition performance of cholic acid-imprinted material prepared with novel surface-imprinting technique. *Polymer* **50**, 3275 (2009).
20. M. Yoshida, Y. Hatate, K. Uezu, M. Goto, and S. Furusaki: Optimization of S-naproxen imprinted polymers: The combination of theoretical and experimental study. *Colloids Surf., A* **169**, 259 (2000).
21. B.J. Gao, J. Wang, F.Q. An, and Q. Liu: Molecular imprinted material prepared by novel surface imprinting technique for selective adsorption of pirimicarb. *Polymer* **49**, 1230 (2008).
22. A. Theis, T.P. Davis, M.H. Stenzel, and C. Barner-Kowollik: Probing the reaction kinetics of vinyl acetate free radical polymerization via living free radical polymerization (MADIX). *Polymer* **47**, 999 (2006).
23. W.A. Braunecker and K. Matyjaszewski: Controlled/living radical polymerization: Features, developments, and perspectives. *Prog. Polym. Sci.* **32**, 93 (2007).
24. H.Q. Zhang: Controlled/"living" radical precipitation polymerization: A versatile polymerization technique for advanced functional polymers. *Eur. Polym. J.* **49**, 579 (2013).
25. A. Kowalczuk-Bleja, B. Trzebicka, H. Komber, B. Voit, and A. Dworak: Controlled radical polymerization of p-(iodomethyl) styrene—a route to branched and star-like structures. *Polymer* **45**, 9 (2004).
26. R. París, B. Mosquera, and J.L. de la Fuente: Atom transfer radical copolymerization of glycidyl methacrylate and allyl methacrylate, two functional monomers. *Eur. Polym. J.* **44**, 2920 (2008).
27. P.V. Mendonça, A.C. Serra, C.L. Silva, S. Simões, and J.F.J. Coelho: Polymeric bile acid sequestrants-synthesis using conventional methods and new approaches based on "controlled"/living radical polymerization. *Prog. Polym. Sci.* **38**, 445 (2013).
28. J. Pietrasik and N.V. Tsarevsky: Synthesis of basic molecular brushes: ATRP of 4-vinylpyridine in organic media. *Eur. Polym. J.* **46**, 2333 (2010).
29. X.X. Li, J.M. Pan, J.D. Dai, X.H. Dai, L.C. Xu, X. Wei, H. Hang, C.X. Li, and Y. Liu: Surface molecular imprinting onto magnetic yeast composites via atom transfer radical polymerization for selective recognition of cefalexin. *Chem. Eng. J.* **198–199**, 503 (2012).
30. J.D. Dai, J.M. Pan, L.C. Xu, X.X. Li, Z.P. Zhou, R.X. Zhang, and Y.S. Yan: Preparation of molecularly imprinted nanoparticles with superparamagnetic susceptibility through atom transfer radical emulsion polymerization for the selective recognition of tetracycline from aqueous medium. *J. Hazard. Mater.* **205–206**, 179 (2012).
31. X. Qiu, X. Ren, and S. Hu: Fabrication of dual-responsive cellulose-based membrane via simplified surface-initiated ATRP. *Carbohydr. Polym.* **92**, 1887 (2013).
32. D.J. Siegwart, J.K. Oh, and K. Matyjaszewski: ATRP in the design of functional materials for biomedical applications. *Prog. Polym. Sci.* **37**, 18 (2012).
33. J. Wood and L.F. Gladden: Modelling diffusion and reaction accompanied by capillary condensation using three-dimensional pore networks. Part 1. Fickian diffusion and pseudo-first-order reaction kinetics. *Chem. Eng. Sci.* **57**, 3033 (2002).
34. Y.S. Ho and A.E. Ofomaja: Pseudo-second-order model for lead ion sorption from aqueous solutions onto palm kernel fiber. *J. Hazard. Mater.* **129**, 137 (2006).
35. P. Brocos, J. Gracia-Fadrique, A. Amigo, and Á. Piñeiro: Application of the extended langmuir model to surface tension data of binary liquid mixtures. *Fluid Phase Equilib.* **237**, 140 (2005).
36. N. Chilton, N.J. Losso, E.W. Marshall, and M.R. Rao: Freundlich adsorption isotherms of agricultural by-product-based powdered activated carbons in a geosmin–water system. *Bioresour. Technol.* **85**, 131 (2002).

https://doi.org/10.1557/jmr.2013.256 Published online by Cambridge University Press

37. V.I. Smirnov and V.G. Badelin: Enthalpies of solution of β-alanyl-β-alanine in aqueous solution of amides at 298.15K. *Thermochim. Acta* **536**, 74 (2012).
38. D.V. Demidov, I.V. Mishin, and M.N. Mikhailov: Gibbs free energy minimization as a way to optimize the combined steam and carbon dioxide reforming of methane. *Int. J. Hydrogen Energy* **36**, 5941 (2011).
39. L. Song, S. Wang, C. Jiao, X. Si, Z. Li, S. Liu, S. Liu, C. Jiang, F. Li, J. Zhang, L. Sun, F. Xu, and F. Huang: Thermodynamics study of hydrogen storage materials. *J. Chem. Thermodyn.* **46**, 86 (2012).
40. W.Z. Xu, W. Zhou, P.P. Xu, J.M. Pan, X.Y. Wu, and Y.S. Yan: A molecularly imprinted polymer based on TiO_2 as a sacrificial support for selective recognition of dibenzothiophene. *Chem. Eng. J.* **172**, 191 (2011).

https://doi.org/10.1557/jmr.2013.256 Published online by Cambridge University Press